Multiconformational States in Phosphoglycerate Dehydrogenase[†,‡]

Jessica K. Bell,[||,§] Gregory A. Grant,[#] and Leonard J. Banaszak*,[||]

Department of Biochemistry, Molecular Biology and Biophysics, University of Minnesota, Minneapolis, Minnesota 55455, and Department of Molecular Biology and Pharmacology and the Department of Medicine, Washington University, St. Louis, Missouri 63110

Received August 15, 2003; Revised Manuscript Received January 23, 2004

ABSTRACT: Phosphoglycerate dehydrogenase (PGDH) catalyzes the first step in the serine biosynthetic pathway. In lower plants and bacteria, the PGDH reaction is regulated by the end-product of the pathway, serine. The regulation occurs through a V_{max} mechanism with serine binding and inhibition occurring in a cooperative manner. The three-dimensional structure of the serine inhibited enzyme, determined by previous work, showed a tetrameric enzyme with 222 symmetry and an unusual overall toroidal appearance. To characterize the allosteric, cooperative effects of serine, we identified W139G PGDH as an enzymatically active mutant responsive to serine but not in a cooperative manner. The position of W139 near a subunit interface and the active site cleft suggested that this residue is a key player in relaying allosteric effects. The 2.09 Å crystal structure of W139G-PGDH, determined in the absence of serine, revealed major quaternary and tertiary structural changes. Contrary to the wildtype enzyme where residues encompassing residue 139 formed extensive intersubunit contacts, the corresponding residues in the mutant were conformationally flexible. Within each of the three-domain subunits, one domain has rotated ∼42° relative to the other two. The resulting quaternary structure is now in a novel conformation creating new subunit-to-subunit contacts and illustrates the unusual flexibility in this V_{max} regulated enzyme. Although changes at the regulatory domain interface have implications in other enzymes containing a similar regulatory or *ACT* domain, the serine binding site in W139G PGDH is essentially unchanged from the wildtype enzyme. The structural and previous biochemical characterization of W139G PGDH suggests that the allosteric regulation of PGDH is mediated not only by changes occurring at the ACT domain interface but also by conformational changes at the interface encompassing residue W139.

D-3-Phosphoglycerate dehydrogenase (PGDH)[1] (*SerA*) catalyzes the first committed step of the serine biosynthetic pathway, oxidizing 3-phosphoglycerate to 3-phosphohydroxypyruvate with the concomitant reduction of NAD to NADH. The product of the PGDH reaction is converted to 3-phosphoserine by *SerC* transaminase and finally dephosphorylated by *SerB* phosphoserine phosphatase to yield serine. This simple pathway in lower plants and prokaryotes is controlled by a feedback mechanism in which the end product of the pathway, serine, is able to allosterically regulate the PGDH reaction (*1*, *2*). The inhibition by serine occurs in a cooperative manner with the first two of four molecules binding with positive cooperativity and the remaining two binding with negative cooperativity (*3*). The inhibitory effect of serine is primarily on the velocity of the reaction rather than the binding of either substrate or cofactor (*4*). Thus, the allosteric effects are classified as following a V-type mechanism rather than the more common regulatory events occurring through changes in K_m.

The crystallographic structure of the PGDH/NAD/serine complex (pdbcode 1PSD) (*5*) revealed a homotetramer with coordinates for residues E7 to Y410, see Figure 1a. In the tetramer, each subunit consisted of three distinct domains, nucleotide binding (NBD), substrate binding (SBD), and regulatory or serine binding (RBD) connected by seemingly flexible polypeptide linkages.

The 222 symmetry of the inhibited PGDH resembled an elongated toroid. The tetramer was unusual in that it contained only two, instead of three, types of major subunit/subunit interfaces. The major subunit interfaces appear between RBDs and the NBDs (*5*). Two adjacent NBDs interlock through primarily hydrophobic interactions between extended loops from each subunit, depicted in Figure 1b. The NBDs in the inhibited crystal structure contained bound coenzyme at the sites shown in Figure 1a. The coenzyme is situated in a cleft between two domains, the SBD in red and NBD in blue. This cleft is exposed to solvent in the serine-

[†] The work contained within this report was funded by a National Institutes of Health grant to G.A.G. (GM056676) and to L.J.B. (GM13925). Use of the Argonne National Laboratory Structural Biology Center beamline at the Advanced Photon Source was supported by the U. S. Department of Energy, Office of Energy Research, under Contract No. W-31-109-ENG-38.

[‡] Atomic coordinates have been deposited in the Protein Data Bank (PDB; http://www.rcsb.org/pdb/; info@rcsb.org) at the Research Collaboratory for Structural Bioinformatics (RCSB; http://pdb.rutgers.edu/) under the pdb code 1SC6.

* To whom correspondence should be addressed. E-mail: banas001@tc.umn.edu. Phone: (612) 626-6597.

[||] University of Minnesota.

[#] Washington University.

[§] Current address: National Institute of Diabetes and Digestive and Kidney Diseases, National Institutes of Health, Bethesda, MD 20892.

[1] Abbreviations: PGDH, 3-phosphoglycerate dehydrogenase; NAD, nicotinamide adenine dinucleotide, oxidized form; NADH, nicotinamide adenine dinucleotide, reduced form; FDH, formate dehydrogenase; asu, asymmetric unit; CNS, crystallographic and NMR systems; LS, method of least squares minimization; RMS or RMSD, root-mean-square distance difference; RBD, regulatory domain of PGDH; NBD, NAD binding domain of PGDH; SBD, substrate binding domain of PGDH.

10.1021/bi035462e CCC: $27.50
Published on Web 03/02/2004

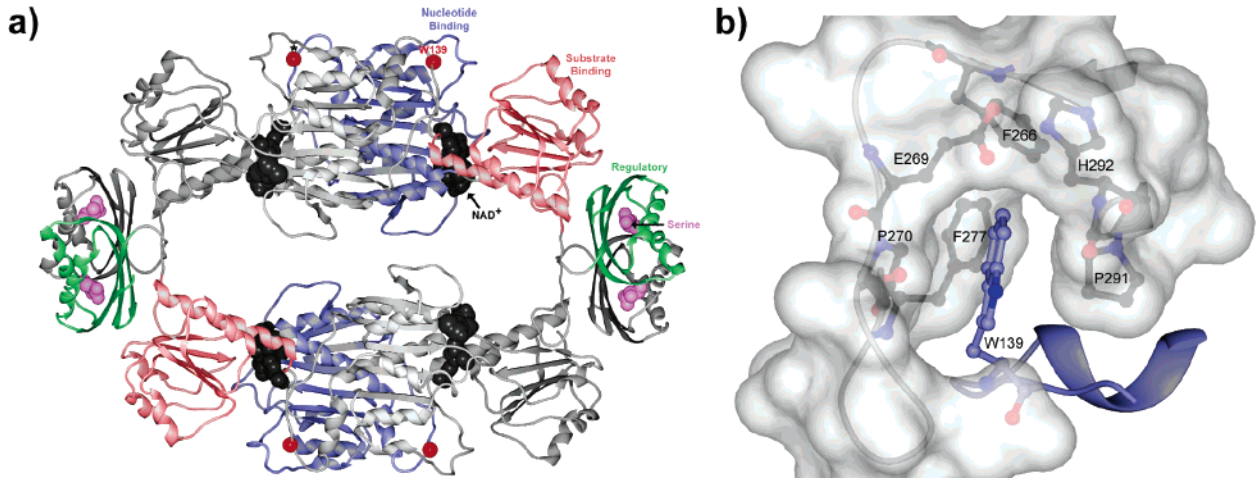

FIGURE 1: Overview of D-3-phosphoglycerate dehydrogenase. (a) Ribbon diagram of PGDH shows the homotetramer with two subunits colored gray and the other two colored by subunit domains. Blue denotes the nucleotide binding domain; red, substrate binding domain; green, regulatory domain. Black spheres represent the bound cofactor, NAD, and purple spheres represent the serine molecules. Red spheres represent the Cα of residue 139. The asterisk denotes the W139 residue shown in detail in panel b. (b) Surface rendering of the W139 binding pocket. The view was generated by rotating panel (a) 90° into the plane of page. Residues encased in the gray surface are from one subunit, whereas the blue ribbon and residue 139 are contributed by the adjacent subunit.

inhibited crystal structure. Insight into the active conformation of PGDH came from structural homology with other D-2-hydroxyacid dehydrogenases having a similar active site cleft. Unlike PGDH, the other family members are dimers lacking the regulatory domains. In this larger family having the linked NBD−SBD fold (*2*, *6*), the dimer interface is formed by essentially the same contacts as the NBD/NBD interface shown in Figure 1a. Lamzin et al. have shown through crystallographic analysis of apo- and holo-formate dehydrogenase that upon binding both substrate analogue and cofactor, the substrate binding domain rotates toward the nucleotide binding domain effectively shielding the active site from bulk solvent (*7*). This observed conformational change in a related enzyme suggested that in the active state, PGDH might undergo a similar movement.

For wildtype PGDH, the interface at adjacent regulatory domains couples to create an extended β-sheet, recently classified as an ACT domain (*8*). Each regulatory interface forms two serine-binding sites, related by 2-fold symmetry as is visible in Figure 1a. The serine molecules (purple spheres in Figure 1a) interact with atoms from both subunits of the interface (*5*). The mechanism by which serine transmits inhibition to the active site, 33 Å away, is unknown but has been postulated to involve the tethering of the regulatory domains together to create a rigid quaternary structure with a solvent-exposed active site cleft (*9*). Potential hinges or pivot points were identified by Grant et al. as Gly−Gly sequences within the polypeptide chain connecting both the nucleotide and substrate domains (Gly^{294}−Gly^{295}) and substrate and regulatory domains (Gly^{336}−Gly^{337}) (*10*, *11*).

To capture the different conformations that PGDH may undergo between its active and inhibited states, we have screened several point mutations for their suitability for structural study. A unique feature of the enzyme is the occurrence of only a single tryptophan residue (W139) that inserts into a pocket in the adjacent nucleotide binding domain (*12*), as is visible in Figure 1b. The tryptophan side chain is also within ~5 Å of the putative His^{292}−Glu^{269} proton relay system of the adjacent subunit. Removing the indole ring of W139 reduces the catalytic activity by 600-fold, but the sensitivity to serine remains essentially unchanged (*13*). However, serine binding studies with the W139G PGDH show that serine no longer binds cooperatively (*13*). Furthermore, this mutation significantly weakens the subunit/subunit contact in this region such that, in solution, the enzyme appears to be in equilibrium between a tetrameric and a dimeric form (*13*). The uncoupling of serine binding and cooperativity of inhibition suggested that W139 may play a key role in subunit communication.

In this study, we present the structural changes within the W139G mutant, resolved at 2.09 Å resolution, responsible for reduced activity and loss of inhibitory cooperativity. The results described below illustrate the domain/domain flexibility and its consequences on the quaternary structure.

EXPERIMENTAL PROCEDURES

Chemicals of reagent quality were used throughout the study and purchased from Sigma Aldrich unless otherwise noted.

Expression and Purification. The W139G PGDH plasmid (*12*) was transformed into competent SURE cells (Stratagene). This plasmid has background mutations of 4 C/A where the four cysteines per subunit of PGDH have been mutated to alanine. Ten-milliliter LB cultures (150 μg mL^{-1} ampicillin) were grown for 3−5 h at 37 °C to turbidity. Each culture was then transferred to a 1-L flask of 2×YT broth plus antibiotic and grown to an $OD_{600\ nm}$ of 0.6−0.8. Protein expression was induced with 1.5 mM iso-propylthiogalactoside (IPTG). Cultures were grown for 4 h at 37 °C and then harvested by centrifugation at 3000 rpm for 20 min. Cell pellets were resuspended in 50 mM KH_2PO_4, pH 7.0, 2 mM DTT, 1 mM EDTA, and 0.05% NaN_3 [buffer A] and sonicated to lyse the cells. The remainder of the purification protocol is described in ref *14*. Purified protein was concentrated using a Centriprep 10K [Amicon] and dialyzed against buffer A. Protein was stored at 4 °C.

Seleno-Methionine Enriched Expression. The W139G vector was transformed into B834 (de3) competent cells (Novagen). Ten-milliliter 2×YT cultures (150 μg mL^{-1}

ampicillin) were grown overnight at 37 °C. The cells from the overnight cultures were spun down and washed twice in M9 media. The M9 media contained (in addition to 0.5 g of NH_4Cl, 1.5 g of KH_2PO_4, 3 g of Na_2HPO_4 per L) 2 mM $MgSO_4$, 0.025 g of $FeSO_4 \cdot 7H_2O$, 0.4% glucose, 0.4 mg mL^{-1} of all amino acids except methionine, 1 mg mL^{-1} vitamin solution (Life Technologies) and 0.4 mg mL^{-1} Se-Met and antibiotic [40 μg mL^{-1} ampicillin] per 1 L total volume. The washed cells were added to 1-L flasks of M9 media. Cells were grown to an $OD_{600\ nm}$ of 1.0 at 37 °C and induced with 1.5 mM IPTG. Cells were harvested after ~12 h by centrifugation at 4 K rpm for 20 min. The protein was purified as described above. The number of seleno-methionines incorporated was determined by comparing electrospray mass spectra (ESMS) of the unenriched to enriched protein. The ESMS studies were done by the University of Minnesota Cancer Research Center's Mass Spectrometry facility.

Dynamic Light Scattering Experiments. Translational diffusion constant measurements were conducted at protein concentrations of 0.5, 1.0, and 2.0 mg mL^{-1} in buffer A. For each concentration measured, the protein was spun at 14 000 rpm for 10 min and passed through a 0.1 μM filter. A 12 μL sample was equilibrated by a built-in thermostat to the desired temperature. Data were collected on a protein solutions dynamic light scattering (DLS) system and evaluated with the DynaPro version 4.0 software. Fifteen to twenty data points were measured for each temperature. The average of these data points was reported for the DLS parameters. Points that were outside one standard deviation were excluded. Data were plotted in Sigma Plot 5.0 Jandel Scientific Inc.

Crystallization. Crystals were grown by the hanging drop method with 3 μL of W139G PGDH (≥10 mg mL^{-1} in buffer A, 2 mM NAD, 5 mM α-ketoglutarate) and 3 μL 0.1 M citrate, pH 5.2, 15−16% PEG 4 K (well solution) at 18 °C. Seleno-enriched and nonenriched crystals grew under the same conditions. Typically crystals grew overnight with diffraction from 2.8 Å (home source) to 2 Å (synchrotron source). The crystals were monoclinic, space group $P2_1$, with four subunits in the asymmetric unit and unit cell parameters of $a = 74.48$ Å, $b = 70.84$ Å, $c = 149.47$ Å, $\alpha, \gamma = 90°$, $\beta = 95.39°$.

Data Collection. Data collected at the Structural Biology Center (SBC), Advanced Photon Source (APS), Argonne National Laboratories, Chicago, IL, was recorded on an SBC APS1 3 × 3 CCD area detector at beamline 19-BM. For each crystal, an X-ray fluorescence scan of the Se-crystals was measured with a Bicron scintillation counter. From the scan, three wavelengths corresponding to the peak (0.97934 Å), inflection point (0.97951 Å), and remote (0.95373 Å) energies were selected for data collection. Complete data sets [total rotation: 185° in Ω, $\phi = 0$ and 180°] were collected at each wavelength. Data were indexed, integrated, and scaled with HKL2000 suite (*15*). Data collection statistics are recorded in Table 1.

Multiwavelength Anomalous Diffraction. The W139G data were input into both SOLVE (*16*) and the software suite Crystallographic and NMR Systems (CNS) versions 1.0 (*17*) for heavy/anomalous atom searches. SOLVE found 24 of the 32 sites. An anomalous difference Fourier map was calculated from the MAD phases and the anomalous data using CNS. The map was displayed at 5σ in O (*18*) and used to identify the remaining eight sites. SOLVE was rerun with the coordinates for all 32 sites input to improve the phases. The FOM was 0.5 at 2.8 Å. Density modification and phase extension (*19*) were applied to improve the phases, FOM = 0.61−2.09 Å. MAID (*20*) was used to build the initial model. Because of poor density for the turn and loops, the bones from MAID were used to superimpose the domains of the native PGDH subunit into the density. After a complete model was built using O, the coordinates were subjected to simulated annealing, positional and B factor refinement using CNS. Model building was continued to improve upon disordered regions and correct side chain rotamers, followed by positional and B factor refinement. Waters were added with the waterpick module of CNS. Cofactor coordinates were taken from the *1psd* structure and modified to fit the electron density. The model was evaluated with PROCHECK (*21*). Refinement statistics are given in Table 1.

Table 1: MAD Data Collection Statistics for W139G D-3-Phosphoglycerate Dehydrogenase

data collection	peak	inflection	remote
wavelength, Å	0.97934	0.97951	0.95373
cell, *a*, Å	74.49	74.56	74.55
b, Å	70.84	70.94	70.96
c, Å	149.47	149.91	149.83
β, °	95.39	95.35	95.38
resolution, Å	2.07	2.07	2.07
completeness, %	98.4	98.1	88
reflections	95387	93182	92509
$\langle I \rangle / \sigma I$	22.9	27.6	10.2
R_{merge},[a] %	8.5	7.5	8.6
F. O. M.			
initial	0.5		
density modified	0.61		
model refinement			
resolution	2.09		
R_{work},[b] %	22		
R_{free}, %	26		
no. of atoms			
protein	12195		
ligand	175		
solvent	472		
RMS deviation			
bond lengths, Å	0.004		
bond angles, °	1.05		

[a] $R_{merge} = (\Sigma|I - \langle I \rangle|)/\Sigma I$ where I is the measured intensity of reflections with indices *hkl*. [b] $R_{work} = (\Sigma||F_o| - |F_c||)/(\Sigma|F_o|)100$ where F_o and F_c refer to the observed and calculated structure factor amplitudes for indices *hkl*, respectively: R_{free} set contained 10% of the total data.

X-ray Model Comparisons. To compare and/or overlay the coordinate results from W139G crystals with those of the inhibited wildtype PGDH, least-squares methods from several software sources were used (*22*) (*Pymol*, DeLano Scientific, Swisspdb). Studies of the domain/domain changes were carried out using the software, *Dyndom* (*24*, *25*). Superpositioning by least squares were done both with a single subunit and a tetramer.

RESULTS AND DISCUSSION

Dynamic Light Scattering. Stability differences between mutant and wildtype enzyme were readily observed in the purified protein. Within days of purification the mutant enzyme would slowly precipitate, whereas the native enzyme remained stable for up to two months at 4 °C in buffer A. Dynamic light scattering experiments and the resultant

translational diffusion constant (D_T) were obtained to estimate the oligomeric state of the mutant enzyme and to define the decrease in stability. WT-PGDH and W139G have similar D_T and polydispersity values between 10 and 30 °C. Between 30 and 35 °C the mutant formed a large aggregate (decreased D_T) indicative of denaturation and/or aggregation (data not shown). The WT enzyme remained monodisperse throughout the temperature range (10−40 °C). W139G PGDH was clearly more susceptible to temperature induced denaturation.

Grant et al. reported that the W139G mutant was in equilibrium between a dimeric and tetrameric species as observed by gel filtration (*13*). The DLS data of the mutant at room temperature compared to the wildtype enzyme is consistent with the W139G enzyme remaining a tetramer. The observations were confirmed at several protein concentrations including 0.5, 1.0, and 2.0 mg mL^{-1}; no change in D_T was observed over this concentration range (data not shown). The polydispersity values (%), 12 ± 1.4 and 15 ± 1.6 for WT and W139G, respectively, indicated that both WT and mutant were monodisperse in these experiments.

Structural Determination. Three complete data sets of anomalous diffraction data at the peak, inflection and remote energies of the selenium absorption edge were collected at SBC-CAT, APS. Data collection statistics are given in Table 1. From a data set collected on the University of Minnesota X-ray equipment, four molecules were assigned to the asymmetric unit [Matthew's coefficient, V_m, 2.2 $Å^3$/Da, solvent content 43.6%] and a screw axis along *b* or *b** [*0k*0 = 2*n*] had been determined.

MAD phasing techniques were used to determine the structure of W139G-PGDH. The positions of the selenium atoms were calculated from the anomalous and dispersive differences of the selenium atoms using the software SOLVE version 1.18 (*16*, *23*−*28*). Electrospray mass spectrometry analysis of the Se-Met W139G protein indicated eight of nine potential methionines had Se incorporated per monomer with the N-terminal methionine probably removed. Given four monomers in the asymmetric unit, the SOLVE program was able to identify 24 of the 32 predicted sites in its initial run.

The starting phases, calculated from the position of the Se atoms with a figure of merit (FOM) cutoff of 0.5, went to 2.8 Å. Solvent flattening, histogram matching, and phase extension were done with the DM program (*19*) within the CCP4 suite version 4.1 (*29*). By these judicious changes in the calculated electron density map and the resulting inverse transform, the phases to 2.09 Å were calculated (FOM_{dm} = 0.61).

Initial fitting of the MAD phased map was done by MAID (*20*). The program was unable to connect many of the secondary structural elements it identified because of poor density at turns and loops. Averaged electron density for the four subunits in the asymmetric unit could not be employed because the hinge angle between the substrate binding and nucleotide binding domains of each subunit differed, as did the position of extended loops in the nucleotide binding domain, discussed below. Using the bones output from MAID, the domains of the native PGDH monomer were placed in the asymmetric unit. The final results from the crystallographic refinement are given in Table 1.

Overall Structure. After an initial round of model building, it was readily apparent that the nucleotide binding domain had undergone a dramatic rotation/translation. The W139G PGDH structure is shown in Figure 2a. The orientation is looking down the same projection and 2-fold rotation axis as was illustrated in Figure 1a. To confirm that the nucleotide binding domain had been correctly traced within the initial map, the selenium sites at residues 220, 221, and 229, all contained in the nucleotide binding domain, were visually inspected in an anomalous difference Fourier map contoured at 5σ and found to agree with the placement of the Cα trace.

The major quaternary and domain changes provided greater insight into the enzyme's flexibility and hinge regions. An approximation to the interdomain conformational changes in W139G-PGDH compared to the native structure and hinge residues were calculated using *Dyndom* (*30*, *31*). *Dyndom* (http://rugmd4.chem.rug.nl/~steve/DynDom/dyndom.home.html) computed the domain structure of a subunit, the residues involved in bending and/or twisting between domains of the subunit in the two quaternary forms (mutant and wildtype) and the general displacement between domains. In this case, the general displacement is characterized by a 41.9° rotation and a 1 Å translation. For a single subunit of WT and mutant PGDH, the NBD displacement is shown in stereo in Figure 2b.

The *Dyndom* analyses also described two hinge regions: (i) F102−F106 (hinge 1) and (ii) T297−Q298 (hinge 2), Figure 2b − Cα colored blue, within the two polypeptide linkers connecting the NBD and SBD (residues 105−109 and 291−300, respectively). The segment from residues 292−299 in the $2F_o - F_c$ electron density map was disordered, suggesting conformational mobility in this region and may reflect multiple hinge angle positions between identical subunits across the crystal lattice. Therefore, the exact residue assignment for hinge 2 by Dyndom may better be stated as falling within this region of disorder, residues 292−299. Previously, a Gly−Gly sequence (residues 294 and 295) between the NBD and SBD had been described as a source of flexibility and potential hinge between these two domains (*11*). The other linker region, residues 105−109, was readily traced in the $2F_o - F_c$ electron density map. Interestingly, both hinge segments are located N-terminal to an α-helix. The two helices are located in the nucleotide binding and substrate binding domains, respectively, pointing in opposite directions.

Subunit Contacts. The X-ray crystal structures illustrated in Figures 1a and 2a indicated major changes at subunit interfaces. The overall result of the rotation/translation of the nucleotide binding domain in each subunit was a quaternary change that now contained new subunit/subunit interactions across the dyad perpendicular to the plane of the drawing in Figure 2a. Analysis of the atoms near the center of the toroid defined both novel electrostatic and hydrophobic interactions stabilizing the W139G quaternary structure. Figure 3c shows the detailed interactions of the blue subunit with two other subunits of the tetramer (red and green). These newly formed interactions include 16 additional hydrogen bonds formed between subunits in the tetramer or four/subunit in the new interface. Two of the four hydrogen bonds are formed between the blue and green subunits (Asn 190 Nδ2 to Gly 174 O and Gly 189 O to Arg 150 Nε and NH1, blue to green subunits, respectively). The remaining two are water-mediated hydrogen bonds between the blue and red subunits (Lys 22 Nζ to Wat 199 to Gln

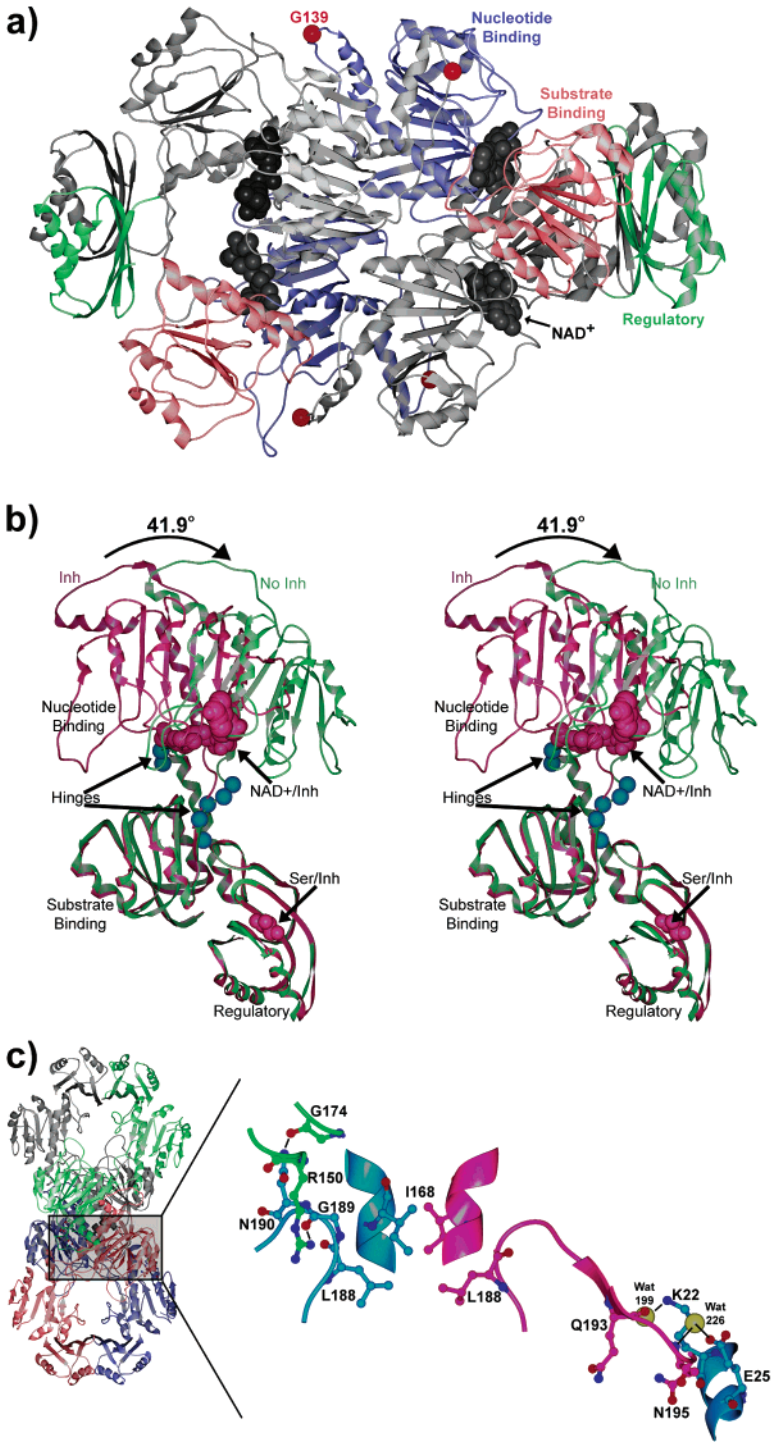

FIGURE 2: Overall architecture of W139G phosphoglycerate dehydrogenase. (a) Ribbon diagram of the quaternary structure of W139G has the homotetramer with two subunits colored gray and the remaining two colored according to subunit domains in the same manner as Figure 1a. Blue denotes the nucleotide binding domain; red, substrate binding domain; green, regulatory domain. Black spheres represent the bound cofactor, and red spheres represent the Cα of G139 in each subunit. (b) Stereoview of a single subunit comparison of serine bound (native) and W139G mutant structure. The purple ribbon depicts the native enzyme with bound NAD^+ and serine shown in purple spheres. The W139G mutant is shown in green ribbon. The hinge residues identified by Dyndom (see text) are highlighted by blue spheres at their Cα's. (c) Subunit contacts across the toroid are shown for W139G. The grayed box over the W139G mutant homotetramer (left) highlights the new subunit contacts shown in detail on the right. The enlarged view depicts hydrogen bonds and hydrophobic interactions in the context of the blue subunit to the red and green subunits (The colors from the tetramer were brightened to help distinguish between subunits.) The gray subunit was excluded as it forms the NBD interface with the blue subunit. Hydrogen bonds are depicted by black solid lines.

193 O and Glu 25 O to Wat 226 to Asn 195 N, blue to red, respectively). At the center of the W139G tetramer, the side chains of residues Ile168 and Leu188 have formed a hydrophobic patch. In the WT structure, the closest distance between residues across the toroid were the symmetrically related Asn190 Nδ2 and Oδ1 atoms at a distance of 5.8 Å.

Nucleotide Binding Domain Interface. At the NBD interface, the domain structure was evaluated for changes in both

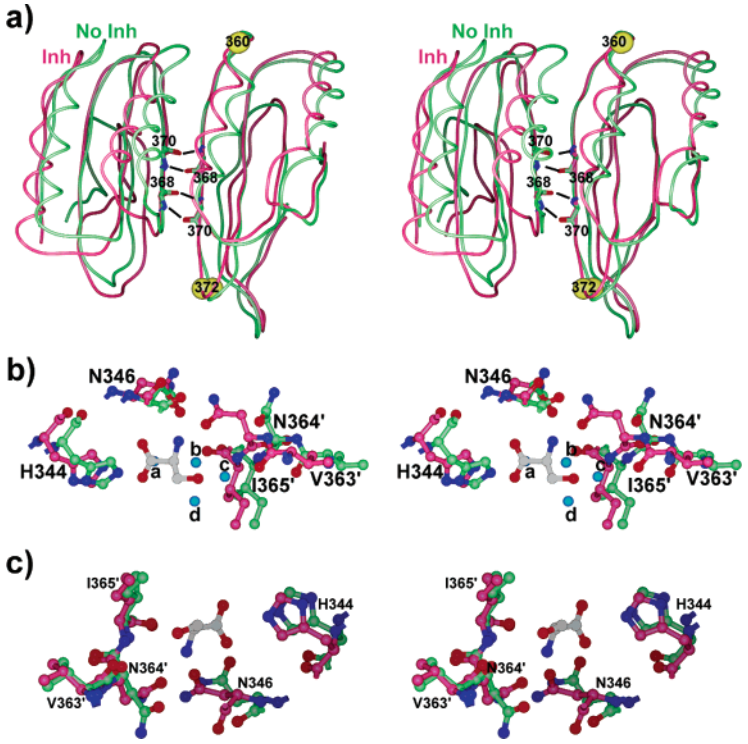

FIGURE 3: Regulatory domain interface and allosteric sites of native and W139G-PGDH. (a) Cartoon diagram of native (purple) and mutant (green) regulatory domains. The stretch of resides from 360 to 372 in each subunit were used for the LS superpositioning, and yellow spheres highlight these residues in one of the two subunits. Interstrand, intersubunit hydrogen bonds are shown by black solid lines. (b and c) Stereo diagrams of the serine binding sites of native (purple Cα's) and mutant (green Cα's) enzymes. Serine bound to the native structure has white Cα's. Blue spheres depict solvent molecules in the W139G allosteric site. Prime indicates residues from the adjacent subunit.

gross conformation and subunit/subunit contacts. A superpositioning of the W139G and WT NBDs (Cα of residues 108−295, excluding residues 141−146 and 265−278) revealed that the overall fold of the domain was unperturbed with an rmsd of 0.83 Å. This is consistent with conformational changes occurring between domains at the flexible hinge regions. The core interactions of the NBD interface remained unchanged with seven hydrogen bonds conserved between mutant and WT.

The extensive contacts between subunits consisting of extended loops (refer to Figure 1b), formed by residues 125−146 of one subunit to residues 264−280 of the adjacent subunit, were partially disordered in the $2F_o - F_c$ electron density maps (typically residues 141−146 and 265−278). This portion of the tertiary structure includes the point mutation at position 139. In the native structure, these two loops form an extensive hydrophobic interaction, as shown in Figure 1b, anchored by W139 and six additional hydrogen bonds between subunits (per subunit). Therefore, although the quaternary change has formed four additional hydrogen bonds per subunit, the disorder observed in residues 141−146 and 265−268 has reduced hydrogen bonds between subunits by six for a net loss of two hydrogen bonds per subunit. The structural rearrangements at the NBD interface and net loss of hydrogen bonds are all consistent with the reduced stability observed in the DLS data and the dissociation of the tetramer into a dimeric species.

Regulatory or Serine Binding Domain Interface. The mutation of W139 to glycine resulted in the loss of cooperativity in serine binding either as observed directly or through catalytic inhibition (*13*). Since the allosteric effects of serine must be transmitted from the RBD/RBD interface, where the effector serine binds, to the active site, the RBD/RBD interface was studied in detail for subtle changes that could be correlated to the biochemical results. Within the RBD interface, there is an eight-stranded β-sheet comprised of four strands from each RBD domain. Using C_α coordinates from the central strands at the interface (residues 360−372) of two subunits, the least squares transformation of the RBD/RBD domains of PGDH and W139G-PGDH was computed and the two experimental segments superimposed. For those 13 Cα carbon atoms, the RMS difference was 0.30 Å, and for all 180 Cα's of the regulatory dimer, the RMS difference was 0.94 Å. The results of the superpositioning are shown in stereo in Figure 3a. By using only these atoms, the relative orientation of hydrogen bonds bridging strands and subunits could be evaluated.

The hydrogen-bonding interactions marked by solid lines in the stereo-drawing of Figure 3a appear virtually superimposable. Hence, no obvious change in the angular properties of the four N−H- - -O═C bonds at the interface between RBDs was observed. Even the hydrogen-bond distances agree to within ±0.05 Å—well beyond the experimental error in the X-ray coordinates. Subject to the limitation of comparing W139G and WT PGDH, the binding of serine does not appear to produce a new stereochemical relationship between the four strands of one RBD with its neighbor at the interface.

Allosteric Sites. To study the allosteric inhibitor sites, the conformational overlays were the same as those used above in the comparison of interstrand, intersubunit hydrogen bonds between adjacent RBDs. The biochemical analyses of serine binding and inhibition with the W139G enzyme reported an

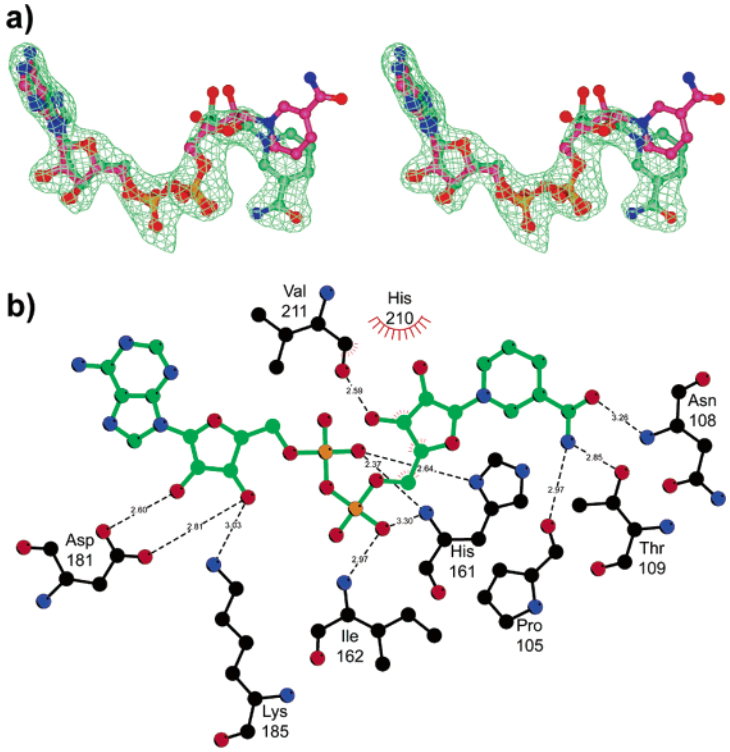

FIGURE 4: W139G cofactor binding site. (a) Stereoview of the NAD bound to W139G (green atoms) and native enzyme (purple atoms). $2F_o - F_c$ electron density (green cage) contoured at 1σ surrounds the W139G cofactor. (b) Ligplot diagram of the W139G cofactor and its hydrogen bond and hydrophobic interactions. Cofactor carbon atoms and bonds are colored in green. W139G carbon atoms and bonds are colored in black. Hydrogen bonds are shown with black dotted lines. Hydrophobic contacts are shown by the red spikes along with their directional properties.

IC_{50} similar to the WT enzyme (12 versus 10 μM, respectively) but a loss of cooperativity in both inhibition of catalysis and binding (*13*). Although no serine was added in the crystallographic studies of W139G PGDH, we have compared the three key residues (H344, N346, and N364′) that interact with the effector between the W139G PGDH structure and the inhibited structure. The results are shown in stereo in Figure 3b,c.

The inhibitor binding site constellation appears to have undergone minor changes in the W139G structure with slight variations at the two RBD/RBD interfaces visible. At both RBD interfaces, one serine binding site (Figure 3b) was filled with a hydrogen bonded solvent network, while there was no evidence for water molecules at the second serine binding site (Figure 3c). Of the three key side chain/effector interactions only the position of the H344 side chain in both sites has not changed in the mutant, and hence might be expected to behave similarly in the W139G with bound serine. The N346 side chain remains in the effector binding site but now forms alternative hydrogen bonds to mainchain carbonyls of residue 373 or 376. The side chain of N364′ has moved out of the serine binding site and is now exposed to bulk solvent. Interestingly, the solvent-exposed position of N364′ in W139G-PGDH may offer an opening into the serine binding site. Once occupied by ligand, the aperture size would then be reduced through the hydrogen bonds between the carboxamide of N364′ and the effector.

The Active Site. W139G-PGDH has reduced activity estimated as an approximately 600-fold decrease in V_{max} (*12*). In addition, Grant et. al have shown that enzyme activity decreases in a linear fashion with the volume of position 139's side chain (*12*). The reduced activity was attributed to disruption of the His/Glu pair by the destabilization of the W139 hydrophobic pocket as shown in Figure 1b.

The active site in the crystals of W139G-PGDH was compared to the active site in the inhibited wildtype enzyme. The superpositioning of the coordinates was done by the method of least squares using the Cα carbons of residues 108−130 and 145−275. The resulting RMSD was 2.0 Å. This comparison left the atoms of the coenzyme in virtually identical positions except for the nicotinamide ring. As can be seen in Figure 4a, the nicotinamide ring in W139G-PGDH has rotated ∼180° around the glycosidic bond; it has moved from the anti to the syn orientation and is now pointing away from the catalytic pocket. The new orientation is stabilized by hydrogen bonding interactions with residues 105, 108, and 109 as shown in Figure 4b. In particular, the carboxamide nitrogen now forms hydrogen bond interactions with the Oγ of T109 (d = 2.85 Å) and the carboxyl of P105 (d = 2.97 Å), the carboxamide oxygen interacts with the amide backbone of N108 (d = 3.26 Å). The adenine portion of the cofactor retains hydrogen bonding contacts identical to the native structure.

PGDH has been shown to be A-side (anti position) specific for hydride transfer (*32*). Yet, the cofactor conformation in the crystal structure of W139G-PGDH closely resembles the orientation of the cofactor in crystalline glyceraldehyde-3-phosphate dehydrogenase, a B-side specific enzyme. Hydride transfer specificity of GAPDH was investigated by Corbier et al. (*33*) and, more recently, by Eyschen et al (*34*, *35*). In these studies, invariant residues responsible for coordinating the carboxamide and orienting the nicotinamide ring for efficient catalysis were systematically mutated (*33*−*35*). Using these altered enzymes, they were able to show that

the NAD moiety bound in both the syn [B-side] and anti [A-side] conformations of the nicotinamide ring (*35*), but no A-side specific catalysis was observed; the enzyme remained B-side specific. Extrapolating to the NAD bound in crystalline W139G-PGDH, the reorientation of the nicotinamide ring may be a contributing factor to the reduction in steady-state activity.

Beyond the reorientation of the redox center of NAD, other conformational factors were also observed. Within the mutant active site, the catalytic constellation of atoms (H292, E269, R240) is almost completely disordered. This is not surprising since the mutation was located but 5 Å from the proton relay system of H292 and E269. Taking into account the nicotinamide effect and the reduced order in the active site, the changes in catalytic properties seem reasonable.

CONCLUSIONS

Of the 146 PGDH sequences currently available (Swissprot, http://us.expasy.org/sprot/) all but 13 contain a tryptophan at position 139 and 9 of those 13 are conservative replacements such as phenylalanine or tyrosine. The highly conserved tryptophan resides in an extended loop, residues 136−146, that forms contacts with residues 260−280 of the adjacent subunit within the NBD interface of PGDH, as illustrated in Figure 1b. The unique positioning of the tryptophan ring at position 139 appears key to maintaining the stability of the tetrameric toroid in the presence of the allosteric inhibitor serine, the T-state, and may play a role in modulating the conformation of the active site residues. As shown schematically in Figure 5, this 222 symmetrical molecule has the unusual property of lacking significant subunit/subunit contacts between A and C or A and D subunits (and the symmetry equivalent interactions). By changing the interaction between the A and B subunit in the W139G mutant, we have observed a new configuration for PGDH, one in which the toroidal structure is twisted into a novel quaternary form. The resulting enzyme is still partially active and can be inhibited by serine but not in a cooperative manner. Because of this mutant's noncooperative inhibition by serine, we believe that the flexibility observed in the W139G structure portends a significant feature in the conformational transition from active to inhibited conformation and have therefore labeled the W139G tetramer as R′. This conformational transition, as presented in this study, clearly involves both domain/domain alterations as well as new subunit interactions mediated by rotation at a molecular hinge.

The precise conformational differences at the NBD/NBD interface are difficult to define due to the disordering of the extended loops in the electron density, consistent with the loops sampling several conformations. Using the approach and software developed by Hayward and Berendsen, the changes in the orientation of the domains as shown schematically in Figure 5 appear to be unequivocally identified (*30*, *31*). The NBDs are rotated ~42° with respect to the RBD−SBD domains. The reduced contacts at this interface clearly contribute to the enzyme's ability to rotate the NBD domains relative to the SBDs and RBDs. Biologically, the loss of W139 interactions could not readily occur, but the in vitro simulation emphasizes the importance of these hydrophobic interactions for both the stability of the enzyme and the cooperative effects of serine. The crystal structure described here suggests that in vivo perhaps more subtle changes at the NBD interface transmit the effects of serine binding.

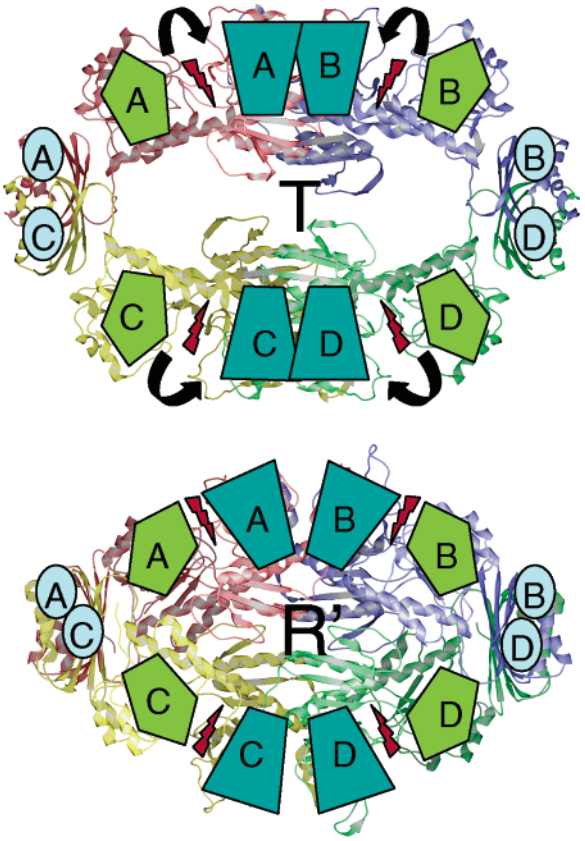

FIGURE 5: Model of the T to R′ transition in PGDH. Enzyme is shown in ribbon form with geometric shapes overlaid on subunit domains (blue trapezoid, nucleotide binding domain; green pentagon, substrate binding domain; cyan circle, regulatory domain). Active site clefts are marked by red lightning bolts. Blacks arrows indicate the domain movement occurring during the transition from the T to R′ state.

Our original hypothesis of allosteric regulation, based upon the serine-inhibited enzyme, proposed that the inhibition, or release of inhibition, would be triggered by the orientation of the regulatory domain β sheets relative to one another across the subunit interface. In the W139G structure, we were able to correlate loss of cooperative serine binding and inhibition to changes, not at the RBD interface, but rather at the NBD interface. So, although we still believe that serine binding or release causes a subtle change at the RBD interface that is propagated to the active site, we can now add that the cooperative inhibition occurs through concerted conformational changes including the NBD interface. We are currently studying the helices flanking the regulatory domain β sheet as a potential propagator of the transition from active to inhibited enzyme.

The W139G mutant has offered insight into the potential conformational changes possible in PGDH brought on by ligands binding to the NBD. The loss of subunit contacts by the extended loop regions coincided with the loss of cooperativity of serine binding and inhibition (*14*) and reduction in stability. The comparison between the inhibited wildtype enzyme and the uninhibited W139G-PGDH lead us to hypothesize that the regulation may occur by serine

binding at the RBD−RBD interface that in PGDH influences the conformational state of the NBD−NBD interface leading to cooperative inhibition.

ACKNOWLEDGMENT

We acknowledge Judy Bratt (University of Minnesota, Minneapolis, MN) for assistance in protein purification and crystallization trials. We are deeply grateful to Ed Hoeffner for maintenance of the University of Minnesota X-ray equipment and computational support. We thank Peter Vallarta of the Mass Spectrometry Facility at the University of Minnesota Cancer Center for enzyme mass determinations. The authors acknowledge the valuable contributions of Andrzej Joachimiak and Rongguang Zhang in securing synchrotron time on the 19-BM line of SBC-CAT and assisting in the MAD data collection. The Minnesota Supercomputing Institute generously supported computations necessary for the X-ray crystallographic model building and analysis.

REFERENCES

1. Dubrow, R., and Pizer, L. (1977) Transient kinetic and deuterium isotope effect studies on the catalytic mechanism of phosphoglycerate dehydrogenase. *J. Biol. Chem. 252*, 1539−1551.
2. Grant, G. (1989) A New Family of 2-Hydroxyacid Dehydrogenases. *Biochem. Biophys. Res. Commun. 165*, 1371−1374.
3. Grant, G. A., Schuller, D. J., and Banaszak, L. J. (1996) A Model For the Regulation of D-3-Phosphoglycerate Dehydrogenase, a V-Max-Type Allosteric Enzyme. *Protein Sci. 5*, 34−41.
4. Sugimoto, E., and Pizer, L. (1968) The mechanism of end product inhibition of serine biosynthesis I. Purification and kinetics of phosphoglycerate dehydrogenase. *J. Biol. Chem. 243*, 2081−2089.
5. Schuller, D. J., Grant, G. A., and Banaszak, L. J. (1995) The allosteric ligand site in the Vmax-type cooperative enzyme phosphoglycerate dehydrogenase. *Nat. Struct. Biol. 2*, 69−75.
6. Lamzin, V., Aleshin, A., Strokopytov, B., Yukhnevich, M., Popov, V., Harytyunyan, E., and Wilson, K. (1992) Crystal structure of NAD-dependent formate dehydrogenase. *Eur. J. Biochem. 206*, 441−452.
7. Lamzin, V. S., Dauter, Z., Popov, V. O., Harutyunyan, E. H., and Wilson, K. S. (1994) High-resolution structures of holo and apo formate dehydrogenase. *J. Mol. Biol. 236*, 759−785.
8. Chipman, D. M., and Shaana, B. (2001) The ACT domain family. *Curr. Opin. Struct. Biol. 11*, 694−700.
9. Al-Rabiee, R., Lee, E. J., and Grant, G. A. (1996) The mechanism of velocity modulated allosteric regulation in D-3-phosphoglycerate dehydrogenase. Cross-linking adjacent regulatory domains with engineered disulfides mimics effector binding. *J. Biol. Chem. 271*, 13013−13017.
10. Grant, G. A., Xu, X., and Hu, Z. (2000) Role of an Interdomain Gly-Gly Sequence at the Regulatory-Substrate Domain Interface in the Regulation of *Escherichia coli* D-3-Phosphoglycerate Dehydrogenase. *Biochemistry 39*, 7316−7319.
11. Grant, G. A., Hu, Z., and Xu, X. L. (2001) Amino acid residue mutations uncouple cooperative effects in *Escherichia coli* D-3-phosphoglycerate dehydrogenase. *J. Biol. Chem. 276*, 17844−17850.
12. Grant, G. A., Kim, S. J., Xu, X. L., and Hu, Z. (1999) The Contribution of Adjacent Subunits to the Active Sites of D-3-Phosphoglycerate Dehydrogenase. *J. Biol. Chem. 274*, 5357−5361.
13. Grant, G. A., Xu, X., and Hu, Z. (2000) Removal of the Tryptophan 139 Side Chain in *E. coli* D-3-phosphoglycerate dehydrogenase produces a dimeric enzyme without cooperative effects. *Arch. Biochem. Biophys. 375*, 171−174.
14. Schuller, D. J., Getter, C. H., Banaszak, L. J., and Grant, G. A. (1989) Enhanced Expression of the *Escherichia coli* serA gene in a plasmid vector. *J. Biol. Chem. 264*, 2645−2648.
15. Otwinowski, Z., and Minor, W. (1997) *Processing of X-ray Diffraction Data Collected in Oscillation Mode*, Vol. 276, Part A, Academic Press, New York.
16. Terwilliger, T. C., and Berendzen, J. (1999) Automated MAD and MIR structure solution. *Acta Crystallogr., Sect. D: Biol. Crystallogr. 55*, 849−861.
17. Brunger, A. T., Adams, P. D., Clore, G. M., Delano, W. L., Gros, P., Grossekunstleve, R. W., Jiang, J. S., Kuszewski, J., Nilges, M., Pannu, N. S., Read, R. J., Rice, L. M., Simonson, T., and Warren, G. L. (1998) Crystallography and NMR System − a New Software Suite For Macromolecular Structure Determination. *Acta Crystallogr., Sect. D: Biol. Crystallogr. 54*, 905−921.
18. Jones, T., Zou, J., Cowan, S., and Kjeldgaard. (1991) Improved methods for building protein models in electron density maps and the location of errors in these models. *Acta Crystallogr., Sect. A: Found. Crystallogr. 47*, 110−119.
19. Cowtan, K. (1994) 'dm': An automated procedure for phase improvement by density modification. *Joint CCP4/ESF-EACBM Newsletter on Protein Crystallogr. 31*, 34−38.
20. Levitt, D. G. (2001) A new software routine that automates the fitting of protein X-ray crystallographic electron-density maps. *Acta Crystallogr., Sect. D: Biol. Crystallogr. 57*, 1013−1019.
21. Laskowski, R. A., MacArthur, M. W., Moss, D. S., and Thornton, J. M. (1993) Procheck: A program to check the stereochemical quality of protein structures. *J. Appl. Crystallogr. 26*, 283−291.
22. Kleywegt, G. J., and Brunger, A. T. (1996) Checking your imagination: applications of the free *R* value. *Structure 4*, 897−904.
23. Terwilliger, T. C., and Eisenberg, D. (1983) Unbiased three-dimensional refinement of heavy-atom parameters by correlation of origin-removed patterson functions. *Acta Crystallogr., Sect. A: Found. Crystallogr. 39*, 813−817.
24. Terwilliger, T. C., Kim, S. H., and Eisenberg, D. (1987) Generalized Method of Determining Heavy-Atom Positions Using the Difference Patterson Function. *Acta Crystallogr., Sect. A: Found. Crystallogr. 43*, 1−5.
25. Terwilliger, T. C., and Eisenberg, D. (1987) Isomorphous Replacement: Effects of Errors On the Phase Probability Distribution. *Acta Crystallogr., Sect. A: Found. Crystallogr. 43*, 6−13.
26. Terwilliger, T. C. (1994) MAD phasing: treatment of dispersive differences as isomorphous replacement information. *Acta Crystallogr., Sect. D: Biol. Crystallogr. 50*, 17−23.
27. Terwilliger, T. C. (1994) MAD Phasing: Bayesian estimates of Fa. *Acta Crystallogr., Sect. D: Biol. Crystallogr. 50*, 11−16.
28. Terwilliger, T. C., and Berendzen, J. (1997) Bayesian MAD Phasing. *Acta Crystallogr., Sect. D: Biol. Crystallogr. 53*, 571−579.
29. Project, N. C. C. (1994) The CCP4 Suite: Programs for Protein Crystallography. *Acta Crystallogr., Sect. D: Biol. Crystallogr. 50*, 760−763.
30. Hayward, S. (1999) Structural principles governing domain motions in proteins. *Proteins 36*, 425−435.
31. Hayward, S., and Berendsen, H. J. C. (1998) Systematic analysis of domain motions in proteins from conformational change − New results on citrate synthase and T4 lysozyme. *Proteins 30*, 144−154.
32. Winicov, I. (1975) Stereospecificity of Hydrogen Transfer by Phosphoglycerate Dehydrogenase. *Biochim. Biophys. Acta 397*, 288−293.
33. Corbier, C., Clermont, S., Billard, P., Skarzynski, T., Branlant, C., Wonacott, A., and Branlant, G. (1990) Probing the Coenzyme Specificity of Glyceraldehyde-3-Phosphate Dehydrogenases By Site-Directed Mutagenesis. *Biochemistry 29*, 7101−7106.
34. Eyschen, J., Vitoux, B., Rahuel-Clermont, S., Marraud, M., Branlant, G., and Cung, M. T. (1996) Phosphorus-31 Nuclear Magnetic Resonance Studies On Coenzyme Binding and Specificity in Glyceraldehyde-3-Phosphate Dehydrogenase. *Biochemistry 35*, 6064−6072.
35. Eyschen, J., Vitoux, B., Marraud, M., Cung, M. T., and Branlant, G. (1999) Engineered glycolytic glyceraldehyde-3-phosphate dehydrogenase binds the anti-conformation of NAD^+ nicotinamide but does not experience A-specific hydride transfer. *Arch. Biochem. Biophys. 364*, 219−227.

BI035462E